Journal of Physics: Conference Series **247** (2010) 012037 doi:10.1088/1742-6596/247/1/012037

Nano-quasicrystal formation in $Zr_{75}Cu_{20}Pt_5$ Glass Ribbons during Annealing Examined by in-situ SWAXS

H. Okuda[1, 4], Y. Kashitani[1], R. Arao, S.Ochiai[1], J.Saida[2], S.Sasaki[3] and H. Masunaga[3]

[1]Department of Materials Science and Engineering, Kyoto University, Sakyo-ku Kyoto 606-8501 Japan,
[2]Center for interdisciplinary Sciences, Tohoku University, Aoba Sendai 980-8578, Japan,
[3]JASRI Spring8, Kohto, Sayo 679-5198 Japan.

E-mail: okuda@materials.mbox.media.kyoto-u.ac.jp

Abstract. Microstructure evolutions of nano-quasicrystals precipitated in ZrCuPt metallic glass ribbons during annealing has been examined by in-situ small-angle scattering and wide angle diffraction (SWAXS). The time-resolved measurements were made at a photon energy close to the Zr K absorption edge to obtain reasonable balance between transmission and resolution. During annealing the sample in vacuum, increase in SAXS intensity and diffraction peak at medium angle region was observed. The size obtained from SAXS and diffraction almost agreed, suggesting that the precipitation process in the glass ribbon is described by a growth process of single-crystalline nano-quasicrystals. Development of precipitated microstructure was further discussed by comparing SAXS profiles and diffraction profiles.

1. Introduction

Precipitation process in metallic glasses is an interesting subject to understand metallurgical background of the stability of glass state of the bulk metallic glass from kinetic viewpoint of phase transformation. Zr-Cu base alloys, in particular, are well known as an alloy system that exhibits excellent stability, for example, like ZrCuAlNi quaternary alloys[1-4]. Among them, Zr-based alloys containing small amount of noble metals such as Pt have been extensively examined by Saida et al[5-9], since such alloys quite often gives very small nanocrystals as primary precipitates at the first crystallization stage, which eventually transform into metastable microstructure containing crystalline phases without a primary quasicrystalline phase in the late stage of heat treatment. One of the reasons that such precipitation processes of quasicrystals are interesting is that it may reflect inherent local environment of glass to some extent. Namely, if the origin of the stability of Zr-Cu based glasses are explained by their local icosahedral order in the glass or supercooled liquid state, precipitation of quasicrystals observed by small addition of noble metal elements may reflect such local environment. If it is the case, kinetics of nucleation and growth may be different from conventional one observed in precipitation processes of age-hardenable metallic alloys. From this viewpoint, microstructures obtained from SAXS, which gives information on growth kinetics of the quasicrystalline precipitates

[4] To whom any correspondence should be addressed.

as concentration heterogeneities, and that obtained by diffraction spot of quasicrystals which gives information on kinetics of precipitates as viewed from lattice order, are important factors to discuss the characteristic microstructure. Analyzing kinetics of precipitation, which is a standard procedure in metallurgy of crystalline alloys for aluminium and iron alloys, is not easy for these glasses, since materials far from equilibrium are generally sensible to the slight deviation of initial conditions of preparation. Another difficulty for Zr-Cu base alloys is that they easily form oxides with a nanometer scale, which also give a strong small-angle scattering.
In the present work, simultaneous SWAXS measurements were made in-situ in vacuum to avoid such problems.

2. Experimental

The sample ribbons with a molar composition of $Zr_{70}Cu_{25}Pt_5$ used in the present experiment were prepared by single-role melt-spinning by a Cu roll rotating at 40 m/s at the surface. The ribbon with 0.02 mm in thickness and 1 mm in width was placed in the furnace placed at the sample chamber evacuated by a turbo molecular pump to avoid oxidation during annealing. In-situ measurements were made at beam-line 40B2 of Spring8, Hyogo, Japan. SAXS and the diffraction profiles were measured with Rigaku RAXIS VII simultaneously, since the photon energy of the present measurements, 17.99 keV, and large area of Image Plate, 300x300 mm^2, were enough to record SWAXS on the same plate with sufficient resolution. By recording them on the same image plate, it is easy to distinguish SAXS by quasicrystals from SAXS by metastable crystallites or oxide crystallites. This point is very important in the present work, since mixed signals of SAXS from glass or quasicrystals and that from crystalline particles or oxides often lead to erroneous conclusions. The sample was heated with electric furnace installed in the chamber, and SWAXS profiles were recorded every 3 minutes with 150 s of exposure. TEM works by Saida et al.[5,6] shows that quasicrystals are spherical in the present condition.

Figure 1. Experimental set-up of the present *in-situ* measurements. The sample chamber, center, was evacuated by a turbo molecular pump during *in-situ* measurements. The upstream and downstream pipes with lower vacuum were separated from the sample chamber.

3. Results and Discussions

Figure 2 gives the SWAXS profiles obtained for the isothermal annealing at 610 K, which were radially averaged from the two-dimensional intensity pattern. For the melt-spun (as Quenched) state, the SAXS intensity profile shows a monotonic decrease with the magnitude of scattering vector, $q=4\pi \sin(\theta)/\lambda$, where θ is the scattering angle and λ is the wavelength of the incident X-rays. At larger q, the intensities increase with q for all the annealing time, which should be mostly the tail of halo peak at much larger q. The SAXS intensities with approximately $q<1$ nm^{-1} increase with annealing time, suggesting that size and volume of the precipitates increase with time. In the larger q region at q~6

nm^{-1}, a Bragg peak was observed, which grows with annealing time. An enlarged figure of the peak is also shown in Fig.2. It is seen that the peak also grows with annealing time, corresponding to the increase in the SAXS intensity.

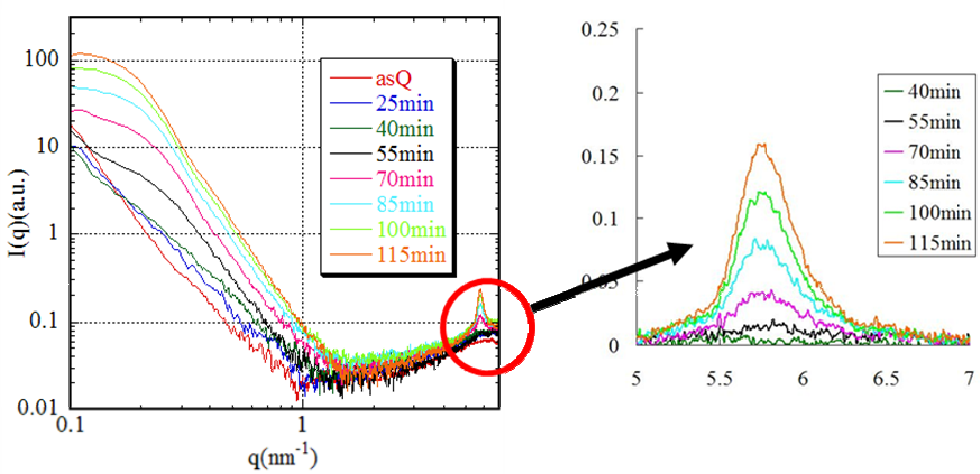

Figure 2. SWAXS intensity of ZrCuPt ribbon annealed at 610 K

Comparing the SAXS part in Fig.2 with SAXS profiles commonly observed for annealed metallic alloys where precipitation hardening is used for designing performance of the materials[10,11], we may notice that interparticle interference peak is not observed in the present sample, which is rather commonly observed for the alloys such as Al-Zn, Al-Zn-Mg or Al-Li[10-12], even for Al-4at%Zn with expected volume fraction of about 3%. This means that the number density of the precipitated quasicrystal is small even in the later stage of annealing where well-defined SAXS profile is observed. The diffraction peak observed at large q also grow with time, suggesting that the growth of quasi-crystalline precipitates. To obtain more quantitative parameters, temporal evolution of the peak intensity for SAXS and diffraction was plotted in Figure 3. When the temporal evolution of SAXS peak intensity and the diffraction peak intensity agree, it suggest that the microstructure of the sample is well approximated by two-phase model, a precipitate having well-defined interface, with a constant concentration contrast between inside and outside of the precipitate and a uniform single-(quasi)crystalline structure in the precipitates. From Fig. 3, the temporal power law for the SAXS was about 5.3 for the intermediate time range as shown in the figure, whereas that for the diffraction is about 3.7. The fact that the temporal powers for the SAXS and the Bragg do not agree each other suggests that the microstructure of the precipitate is not described by a simple two-phase model with a

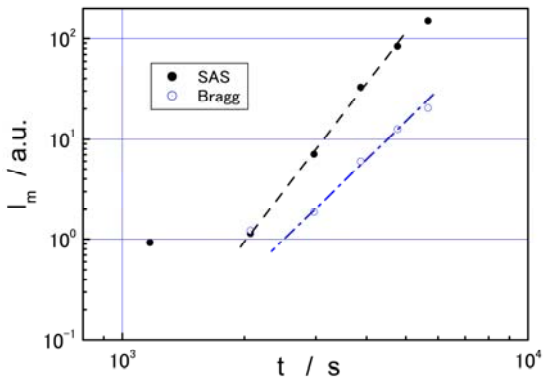

Figure 3. Temporal evolution of the peak intensity for SAS and the diffraction peak at q=5.8 nm^{-1}

fixed structure. To add with, the power is much larger than the ones known for precipitation[13-15]. These results suggest that the precipitation process in the present glass system is different from the precipitation kinetics commonly known for crystalline alloys. Since no interparticle interference is observed in the present SAXS profile, the peak intensity for SAXS is related to $\Delta\rho^2\langle v^2\rangle N$, with $\Delta\rho$ the difference of electron density between the precipitates and the matrix, $\langle v\rangle$ the volume of the precipitates and N the number density of precipitates. When a two-phase model applies for the precipitate microstructures, increase in I_0 is explained by the increase in the volume, number density, or the contrast.

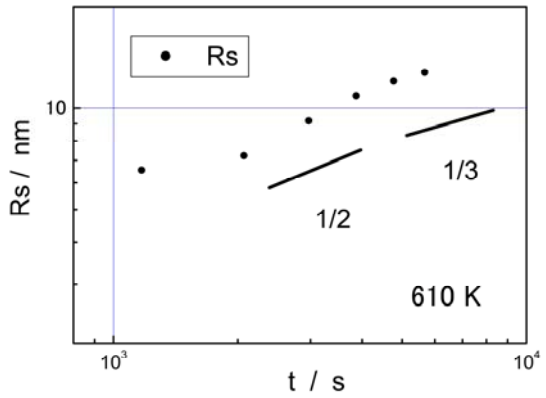

Figure 4. Change of radius, Rs, during annealing.

Figure 4 shows the temporal evolution of spherical radius, Rs, obtained by the Guinier approximation of SAXS profiles. In the initial stage with low scattering intensity, Rs is affected by the SAXS intensity originated from quenched-in fluctuation observed even for as melt-spun sample shown in Fig. 2. In the later stage, however, it is noted that the slope is larger than one half, suggesting that the temporal power law for the growth kinetics is larger than the one expected by the diffusion limited growth[16]. This point is an interesting feature of the quasicrystal growth found in the present experiment, since in most of precipitation processes in crystalline alloys, the temporal power law is one half, or sometimes smaller owing to competitive growth/coarsening or slowing down due to strain effect.

The growth kinetics, i.e., the temporal evolution of the size of quasicrystal is important information as discussed above. In the present measurements, two other parameters on the size of precipitates can be calculated. One is the radius calculated from the Porod regions[17-19], and the other is the one from

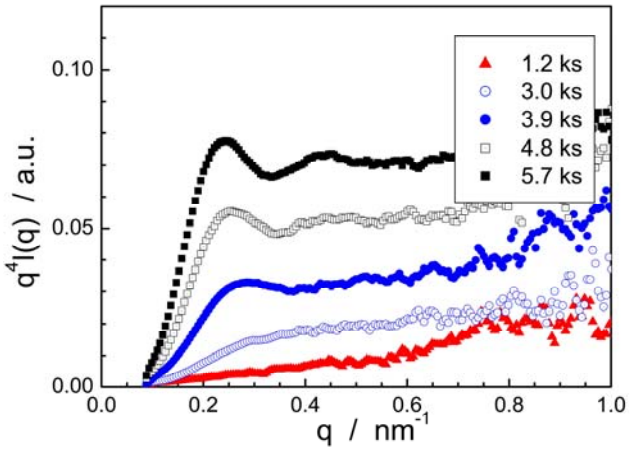

Figure 5. Change of $q^4I(q)$ as a function of q.

the Bragg peak[20]. Assuming that the precipitates are spherical, SAXS intensity from monodisperse size distribution with size R gives a well-defined oscillation with a period that converges to qR= π as q goes to infinity when $q^4I(q)$ is plotted against q. With a broader size distribution, the oscillation of the function, $q^4I(q)$ becomes smaller in amplitude, and the degree of such oscillation is used for the calculation of size distribution from measured SAXS intensity[19]. In other words, such function is a measure of the sharpness of size distribution[21] and also can be used to assess the radius R from the oscillation. Figure 5 gives the function $q^4I(q)$ plotted for several annealing time. It is seen that well-defined first peak is observed in the late stage of annealing. The radius obtained for the first peak of the plot is listed in Table 1. Another size parameter is obtained from the Scherrer analysis of the diffraction peak at q~5.8 nm^{-1}. To obtain the radius of quasicrystallites from diffraction peak, a Gaussian fit of the peak with nonlinear least square fitting was made, and then the size was evaluated by a Guinier approximation. Since the glass matrix is expected in the supercooled fluid state during annealing, we may neglect the effect of strain broadening in the present analysis. The size parameters are summarized in Table 1.

Table 1. Size parameters obtained from the Guinier approximation (Rs), at Porod regions (R_p), and the Scherrer analysis (R_{Bragg})

time / ks	R_s /nm	R_p / nm	R_{Bragg} / nm
1.2	(6.6)	NA	NA
2.1	7.2	NA	NA
3.0	9.2	NA	3.3
3.9	10.9	9.5	6.8
4.8	12.0	10.8	9.0
5.7	12.8	11.2	9.4

In the present analysis, one important point to consider on the diffraction profiles is that these profiles are nearly ideal powder patterns. This is confirmed by the fact that the two-dimensional intensity profiles on the Image Plate give smooth ring patterns for the Bragg peak. Then, we need to treat the diffraction profile as a smeared pattern, since the diffraction profile of a quasicrystallite is smeared by the contribution from small quasicrystals whose Bragg spot is located in the vicinity of that of the quasicrystallite. Figure 6 gives a schematic illustration of a smearing effect at a Bragg position. If only one nanocrystal or a nanoQC contributes to the Bragg spot, then it gives a single crystal pattern. When the effect of coherent strain is negligible, a Bragg profile from a single crystal simply reflects the shape factor of the crystal which is essentially identical to that for SAS, multiplied by the structure factor of the nanocrystal or of the nanoQC. Therefore, an order spot profile of spherical $L1_2$ precipitates

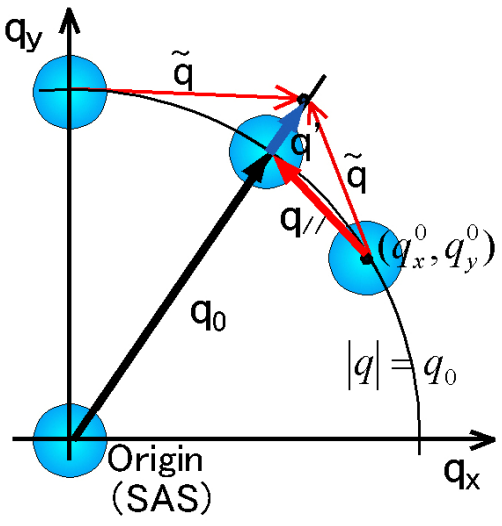

Figure 6. Schematic illustration of the effect of powder pattern on the Bragg profile. The profile in the radial direction is explained by the sum of the contribution from nanoQCs that form the same Debye ring.

in a fcc matrix can be treated in the same manner as that for SAS profile except the interparticle interference function[22]. On the other hand, if the nanoQCs are randomly oriented, a Bragg peak profile across the Debye ring as shown in Fig. 6 is a sum of intensities from nanoQCs contributing to the relevant Debye ring. The Bragg peak profile is then given as

$$I(q') = \int_{|q|=q_0} F^2(\vec{q}'+\vec{q}_{//})P(\vec{q}_{//})dq^2 \quad (1)$$

where $q_{//}$ is the relative distance between the measuring Bragg point and that for other contributing ones shown in Fig.6 and P(q) is an orientation distribution function. Since the Debye ring was uniform and smooth in the present experiment, P(q) can be regarded as a constant. Then eq. (1) is an integration over a sphere of the Debye ring. This equation is equivalent to a smearing calculation for infinite two-dimensional source size as a formality, if the curvature of the Debye ring is negligible compared with the FWHM of the shape factor, i.e., SAS. This is an acceptable approximation in the present experiment, where SAS intensity appears at $q<<1$ nm^{-1} and the Bragg spot appears at $q=5.8$ nm^{-1}. When the area of integration in eq. (1) is replaced from a sphere with $|q|=q_0$ by a plane with $q_z=q_0$, a simple moment calculation gives that the radius obtained from diffraction by Guinier approximation has a statistical meaning of ;

$$R_{Bragg}^{\ 2} = \langle R^6 \rangle / \langle R^4 \rangle$$

and the Porod's law of q^{-4} is changed to q^{-2}. The final slope of q^{-2} for the order spot profile of well-defined $L1_2$ precipitates having powder (polycrystalline) microstructure has been observed in annealed NiAlCr ternary alloys[23]. Considering that Rs is given by

$$R_s^{\ 2} = \langle R^8 \rangle / \langle R^6 \rangle$$

and R_p by

$$R_p = \langle R^3 \rangle / \langle R^2 \rangle$$

the average size should satisfy the relationship

$$R_S > R_{Bragg} > R_p$$

regardless of the shape of the size distribution function. Table 1 shows that this relationship does not hold even for the late stage where well-defined q^{-4} power law is observed for SAXS. The present results suggest that there is a slightly disordered lattice shell outside the quasicrystal precipitates, which may also modify the growth law of the precipitated from a simple diffusion-limited growth. From SAXS results, on the other hand, two phase model is applicable, suggesting that this slightly disordered shell should have the identical composition as that of the inner core, since the oscillation periodicity in Fig. 5 should be otherwise destroyed.

4. Conclusions

Time-resolved measurements of quasicrystal formation from metallic glass ribbons were made for $Zr_{70}Cu_{25}Pt_5$ ternary alloy. The temporal evolutions of the intensity and the radius were examined about composition heterogeneity and the quasicrystalline structure by using SAS and a diffraction spot. Present analysis revealed that the growth kinetic is different from ordinary diffusion-limited growth, and it may stem from the microstructure characteristics of the precipitates, i.e., less lattice-ordered structure of the shell region. Further examination of the structure by using contrast variation with anomalous scattering at the Zr K edge is now in progress.

references

[1] Inoue A, Zhang T and Masumoto T, *Mater. Trans*. 31(1990)17.
[2] Inoue A, *Acta Mater.* 48(2000)279.

[3] Perker A. And Johnson W J, *Appl. Phys. Lett*., 63(1993)2342.
[4] Okuda,H, Murase I, Kurosaki R, Nakagawa E, Ochiai S, Yokoyama Y, Saida J, and Inoue K. *Intermetalics,*14(2006)1038.
[5] Saida J, Matsushita J and Inoue A, *J. Alloys Compd*., **342**(2000) 18.
[6] Saida J. Sanada T, Sato S , Imafuku M and Inoue A, *Appl. Phys. Lett*., **91** (2007) 11901.
[7] Murty B S, Ping D H, Ohnuma M and Hono K, *Acta Mater*. **49**(2001)3453.
[8] Murty S, Ping D H Hono K and Inoue A, *Scr. Mater*. **43**(2000)103.
[9] Okuda H, Fukumoto T, Saida J Ochiai S, Sasaki S and Masunaga H, *J. Appl. Cryst*. **41**(2008)675.
[10] Bauer R and Gerold V, *Acta Metall*., **10**(1962) 637.
[11] Cocco G, Fagherazzi G and Schiffini L, *J. Appl. Cryst.*, **10**(1977)325.
[12] Beddoe R E, Gerstenberg K W and Gerold V, *Decomposition of Alloys, the early stages*, Pergamon Press, Oxford,1984, p110.
[13] Gunton J D, San Miguel M and Sahni P S, *Phase Transition and Critical Phenomena*, vol.8 ed. Domb C and Lebowitz J L, Academic Press, NY,1983 p267.
[14] Hennion M, Ronzaud D and Guyot P, *ActaMetall* **30** (1982)599.
[15] Binder K, Kalos, K and Lebowitz J L, *Adv. Coll. Interf. Sci*., **10** (1979)173.
[16] Doherty,R. D. *Physical Metallurgy*, 2nd ed., ed. Cahn R. and Haasen, P. Chapt. 14, p966.
[17] Porod G, *Kolloid -Z*., **124**(1951)83
[18] Feign L A and Svergun D., *Structure Analysis by Small-Angle X-ray and Neutron Scattering*, Plenum, NY,(1987) p230.
[19] Lechter J H and Schmidt P W, *J. Appl. Phys*. **37**(1966),649.
[20] Culity B D, *Elements of X-ray diffraction*, Addison & Wesley,Reading (1978) p102.
[21] Okuda H, Osamura K and Amemiya Y, *Trans. JIM* **34**(1993) 758.
[22] Okuda H, Tanaka M, Osamura K, and Amemiya Y. *J. Appl. Crystallogr*. **30**(1997)592.
[23] Bley, F, Livet F., Okuda H. and Simon J.P *J. Appl. Crystallogr*. **30**(1997)914.